A Capacitance Estimation Method for DC-Link Capacitors in Railways Based on Precharging Model and Low Sampling Frequency

Xun Wu, *Member, IEEE*, Kaidi Li, Rui Tian, Hengyi Yin, Tianjian Yu, Shu Cheng, and Chunyang Chen

***Abstract*—A dc-link capacitor is an important device and the vulnerable electronic part of the train converter. The capacitance decline of the dc-link capacitor is accelerated because of the influence of voltage, current, charge–discharge frequency, temperature, and other factors. This will lead to circuit performance degradation and even capacitor failures. Therefore, the capacitance estimation of dc-link capacitors is necessary and of great significance to the safe operation of the train. However, the voltage sensors used in the train converter have large noise and low sampling frequency, which makes it difficult to obtain accurate capacitance estimations with existing methods. In this article, an effective capacitance estimation method is proposed to solve these problems. The precharging process is analyzed and an estimation model is built to weaken the impact of the sensor noise. Based on the model, a three-stage iteration algorithm is used for capacitance estimations, which can effectively search for the optimal solution at a low sampling frequency and further reduce the noise influence. The proposed method was verified on a metro vehicle and compared with other algorithms. The experimental results show that the aforementioned problems can be well solved by the proposed method and the estimation error is within 2%.**

***Index Terms*—Capacitance estimation, dc-link capacitor, noise, precharging.**

I. Introduction

THE dc-link capacitor plays an important role in train converters. It is mainly used to absorb the pulsating current, control the ripple voltage, and reduce the impact of overvoltage on switching devices. A film capacitor is widely used in dc-links because of the large capacity, long service life, and low impedance. However, it is still one of the weakest parts in the converter system even though its performance has been greatly improved [1], [2], [3].

Because of the voltage, current, charge–discharge frequency, temperature, and other factors, the life of the capacitor began to decline after a few months. Under hard-working conditions, the aging of the capacitor is accelerated, and its actual life is greatly different from the data in the manufacturer's manual. The capacitor must be replaced to ensure the performance of the converter when the capacitance drops to a certain value. Therefore, the accurate estimation of capacitance is extremely important for the dc-link capacitor and is also the basis of capacitor life prediction methods [4], [5], [6], [7], [8].

Currently, researchers have proposed different capacitance estimation methods. These methods have their own characteristics and can be divided into several groups.

Current injection is an intrusive method for capacitor condition monitoring, which needs to inject a small current signal into the system and uses the response of the system for calculation. For example, the currents at various odd harmonic frequencies [9] can be injected into the solar inverter when it is shut down at night. Then, the dc-link capacitor impedances at various frequencies are evaluated by the current and voltage, and the states of the capacitor can be estimated by the least-mean-square algorithm. For the three-phase inverter, the response of the system is reflected by the dc voltage and three-phase currents, and the capacitance can be obtained by a resonator proposed in [10]. However, these kinds of methods are not suitable for railway applications because they are limited by the IEEE standard and may bring unknown risks to the system.

LC resonance is also used in the capacitor parameter estimations, which usually have high requirements on the detection devices or the parameters of the circuit. The damping characteristics of the capacitor switching-ring is used in [11] for capacitor parameter estimation, in which an extra high-frequency sensor is necessary to monitor the intrinsic high-frequency resonance for calculation. The *LC* resonance can also be achieved by the discharge of the capacitor to the motor [12], and the capacitance can be obtained by measuring the rising part of the resonance current. But it has to adjust the discharge circuit and the control and may also affect the motor performance.

Manuscript received 22 June 2023; revised 24 August 2023; accepted 29 September 2023. Date of publication 9 October 2023; date of current version 6 December 2023. This work was supported by the National Natural Science Foundation of China under Grant 52202428. Recommended for publication by Associate Editor H. Li. *(Corresponding author: Tianjian Yu.)*

Xun Wu, Tianjian Yu, Shu Cheng, and Chunyang Chen are with the School of Traffic & Transportation Engineering, Central South University, Changsha 410075, China (e-mail: xun.wu@csu.edu.cn; yutianjian@csu.edu.cn; 6409020@qq.com; cychen999@csu.edu.cn).

Kaidi Li is with the Shenzhen Metro Group, Shenzhen 518000, China (e-mail: likaidi@shenzhenmc.com).

Rui Tian is with the State Grid Hunan Extra High Voltage Substation Company, Changsha 410002, China (e-mail: 315684379@qq.com).

Hengyi Yin is with the School of Electrical and Computer Engineering, McGill University, Montréal, QC H3A 0G4, Canada (e-mail: hengyi.yin@mail.mcgill.ca).

Color versions of one or more figures in this article are available at https://doi.org/10.1109/TPEL.2023.3322699.

Digital Object Identifier 10.1109/TPEL.2023.3322699

Similar to the discharge of the capacitor, the charging process also contains a lot of information related to the capacitor's status. The capacitor parameters can be calculated by the ripple voltages [13] when the dc-link capacitor is in a stable charging process. In addition, the energy variation [14] and the instantaneous power [15] during the energy exchange can also be used for capacitance estimation. However, one of the problems is that the differential of dc voltage may differ greatly from the true value under the influence of sensor noise.

The combination of the ripple current and voltage is also an effective way for capacitor parameter estimations. For the capacitor without the current sensor, its current can be obtained by the input current and output currents of the circuit [16], [17], [18]; then, the capacitance is calculated according to the physical model. When both the current and voltage of the capacitor are monitored by sensors, the parameters can be calculated with the physical model, and the Goertzel algorithm [19] can be used to solve the problem of filtering.

Other algorithms, such as particle swarm optimization [20], recursive least squares (RLS) [21], [22], [23], recursive extended least squares (RELS) [24], wavelet transform [25], [26], [27], [28], short-time Fourier transform [29], variational mode decomposition [30], and low-pass filter [31], [32] can also be combined with the physical models to calculate the capacitor parameters. For example, the RLS algorithm in [21] is used to determine the parameters of the physical model and that in [23] is used as a filter to smooth the output obtained by the physical model. Wavelet transform is adopted in [25] to reconstruct the high-frequency features of the ripple current and voltage in the wavelet subspace; thus, the capacitor parameter estimation can be calculated by the projection coefficients of the current and voltage.

Although various condition monitoring methods have been proposed for dc-link capacitors, there are still two problems that have not been well solved in railway applications.

One of the problems is the low calculation accuracy caused by the noise of voltage sensors. Commonly, the dc-link voltage is about 1500 V in metros and 3000 V in high-speed trains; thus, the absolute error of the voltage sensor may reach to dozens of volts, which is equal to that of the ripple components. Thus, the capacitor parameter estimation methods using voltage signals fail to get accurate results only when high-precision voltage sensors are installed, which undoubtedly increases the economic cost.

The other problem is that the interval of signal sampling is designed to be very long (100 ms) to reduce the pressure of train communication, which means a large part of the key information contained in the signals is lost. Moreover, considering the safe operation, it is usually not allowed to add additional devices or make any modifications to the system, especially on high-speed trains. Therefore, it is important to get accurate estimation results from the sparse data.

To solve these two problems, a capacitance estimation method based on the precharging model and low sampling frequency is proposed in this article. The precharging process is selected for the condition monitoring of the dc-link capacitor. During the sampling interval, the rise of the capacitor voltage is far greater than the noise fluctuation of the voltage sensor, which can effectively reduce the impact of sensor noise on the calculation. Meanwhile, the voltage monitoring in the precharging process does not have high requirements for the sampling frequency, compared with the monitoring of ripple voltage. Then, the precharging model is built and discretized, the capacitance can be calculated once the coefficients of the model are determined. The three-stage structure RLS-LS-LS is utilized to further eliminate the noise effect and find the optimal solution of the coefficients with sparse data. Thus, the accurate estimations of the capacitance can be obtained. Compared with the existing methods, the proposed method can still get accurate estimation results under the condition of large noise and low sampling frequency.

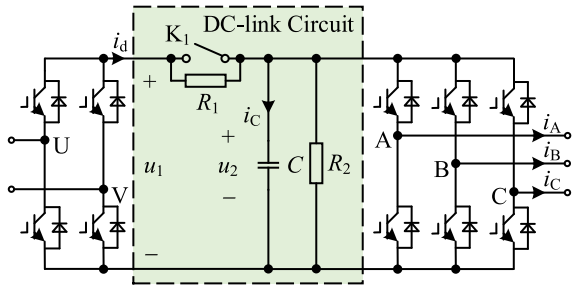

Fig. 1. Topology of a train converter.

The rest of this article is organized as follows. The precharging model and the capacitance estimation algorithm are introduced in Sections II and III, respectively. Section IV shows the verifications and the detailed comparison with existing methods. Finally, Section V concludes this article.

II. DC-Link Capacitor and Precharging Model

A. DC-Link Capacitor in the Train Converter

The topology of a train converter is shown in Fig. 1. The converter is composed of the rectifier, three-phase inverter, and the dc-link circuit. There are two voltage sensors installed in the circuit to monitor the input voltages u_1 and the capacitor voltage u_2. K_1 is a contactor used for precharging, R_1 and R_2 are resistors for precharging and discharging, and C is the dc-link capacitor.

Generally, a film capacitor is used in the dc-link circuit to suppress the ripples and stabilize the dc voltage. It is mainly made of rolled metal electrodes and insulating dielectric film. Fig. 2 shows the exterior, structure, and equivalent circuit of a dc-link capacitor used in high-speed trains. Because the electrode thickness of the film capacitor is only a few microns, its conductive crosssection is relatively narrow. Thus, the parasitic resistance R_C is inevitable although its value is very small, and the film capacitor can be equivalent to the series form of C and R_C.

Similar to other types of capacitors, film capacitor also has problems of aging and failure. The dielectric breakdown and the capacitance loss caused by poor self-healing are the main reasons for the failure of film capacitors. The difference is that the film capacitor commonly has a longer service life, and its capacitance degrades much slower. Fig. 3 shows an accelerated aging test about the degradation of a dc-link capacitor used

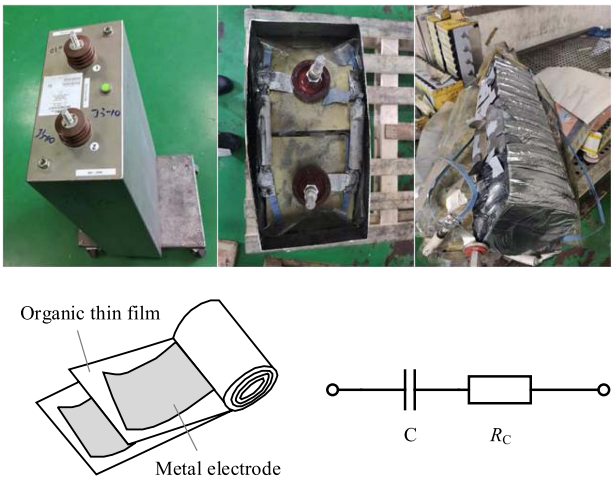

Fig. 2. Exterior, structure, and equivalent circuit of the DC-link capacitor.

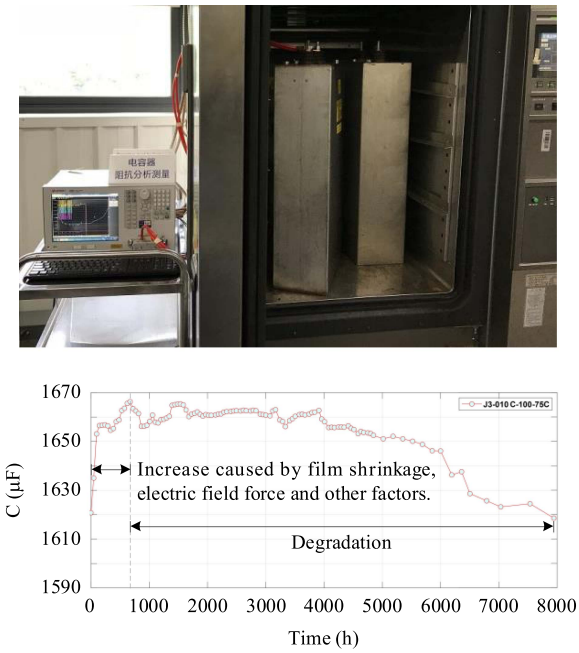

Fig. 3. Degradation of the DC-link capacitor in accelerated aging test (70–75 °C, 1.3/1.5U_N).

in the CRH train; the capacitance decrease is very slow even under high temperature and high-voltage conditions. Therefore, interval capacitance monitoring is acceptable and suitable for the life prediction of dc-link capacitors because it can greatly reduce the power consumption and computational complexity of the monitoring device while eliminating the interference of redundant data. Here, the precharging process is selected for the dc-link capacitor monitoring.

B. Precharging Process and Model

The precharging process is usually executed before the vehicle leaves the depot. During the process, the dc-link circuit is connected to the dc power source while disconnected from the inverter and load. The dc-link capacitor is charged until the voltage difference between u_1 and u_2 is less than 50 V. Then, the contactor K_1 is closed and the inverter is connected to the circuit to start working. Compared with the ripples, the voltage change during the precharging process is more obvious, which is beneficial for suppressing the impact of sensor noise.

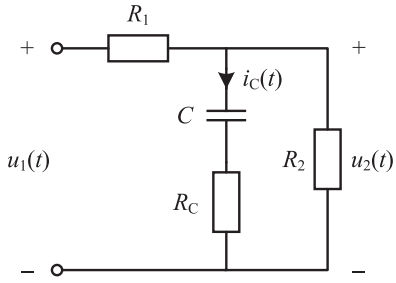

Fig. 4. Equivalent circuit of the precharging process.

During the whole precharging process, the topology shown in Fig. 1 can be equivalent to the circuit shown in Fig. 4. Because the changes of both voltage and current of the dc-link capacitor are monotonic and have no periodic ac component during the process, the applicable frequency range of the equivalent circuit is usually not considered under normal operations. According to Kirchhoff's law, the capacitor current at time t can be obtained as

$$i_C(t) = \frac{u_1(t) - u_2(t)}{R_1} - \frac{u_2(t)}{R_2} = G_1 u_1(t) - G_2 u_2(t) \quad (1)$$

where G_1 and G_2 are constants

$$G_1 = \frac{1}{R_1}, G_2 = \frac{1}{R_1} + \frac{1}{R_2}. \quad (2)$$

In the complex frequency domain, we have

$$U_2(s) = R_C \cdot I_C(s) + \frac{1}{sC} I_C(s). \quad (3)$$

The bilinear transformation is used to decouple the estimations of capacitance and resistance while ensuring the accuracy

$$s = \frac{2}{T} \frac{1 - z^{-1}}{1 + z^{-1}} \quad (4)$$

where T is the sampling time and (3) can be transformed as follows:

$$\left(1 - z^{-1}\right) U_2\left(z^{-1}\right) = \left(b_0 + b_1 z^{-1}\right) I_C\left(z^{-1}\right) \quad (5)$$

$$b_0 = \frac{T}{2C} + R_C, b_1 = \frac{T}{2C} - R_C. \quad (6)$$

It can be seen that the capacitance C can be effectively identified when the parameters b_0 and b_1 are estimated

$$C = \frac{T}{b_0 + b_1}. \quad (7)$$

III. Proposed Capacitance Estimation Method

A. Basic Idea of Capacitance Estimation

As stated earlier, the capacitance can be calculated by b_0 and b_1, thus, the key of the capacitance estimation is the parameter

identifications of (5). Considering the noise $\varepsilon(t)$ of the voltage sensors, the controlled autoregressive and moving average (CARMA) model exists

$$A\left(q^{-1}\right)u_2(t) = B\left(q^{-1}\right)i_C(t) + D\left(q^{-1}\right)\varepsilon(t) \tag{8}$$

where q^{-1} is the delay operator, $A(q^{-1})$, $B(q^{-1})$, and $D(q^{-1})$ are operator polynomials with the order of n_a, n_b, and n_d, respectively.

Usually, the parameters in this model can be calculated by iterative algorithms, such as RLS, RELS, or recursive stochastic Newton algorithm (RSNA). However, these algorithms may have a large estimation bias when the noise is large enough and the data are sparse. Therefore, an algorithm with a three-stage structure is utilized in the proposed method for estimations, which can converge to a better solution. In the first stage, the RLS algorithm is used to estimate the parameters of the equivalent higher-order controlled autoregressive (CAR) model. Then, the parameters of $A(q^{-1})$ and $B(q^{-1})$ are calculated in the second stage. In the third stage, the parameters of the noise are identified. The detailed content is given as follows.

B. Parameter Identification of Fitted High-Order CAR Model

Define $v(t) = D(q^{-1})\,\varepsilon(t)$, we have

$$\begin{aligned}\varepsilon(t) &= D^{-1}\left(q^{-1}\right)v(t), D\left(q^{-1}\right)\\ &= 1 + d_1q^{-1} + \cdots + d_{n_d}q^{-n_d}.\end{aligned} \tag{9}$$

Thus, $v(t)$ can be replaced by the following model:

$$C\left(q^{-1}\right)v(t) = \varepsilon(t), C^{-1}\left(q^{-1}\right) = 1 + c_1q^{-1} + \cdots + c_{n_c}q^{-n_c} \tag{10}$$

where n_c is the order of $C(q^{-1})$. Then, (8) can be written as

$$A\left(q^{-1}\right)u_2(t) = B\left(q^{-1}\right)i_C(t) + v(t). \tag{11}$$

According to (10) and (11), the CARMA model in (8) can be nearly expressed as the following CAR model:

$$\alpha(q^{-1})u_2(t) = \beta(q^{-1})i_C(t) + \varepsilon(t) \tag{12}$$

$$\alpha(q^{-1}) = A(q^{-1})C(q^{-1}), \beta(q^{-1}) = B(q^{-1})C(q^{-1}) \tag{13}$$

$$A(q^{-1}) = 1 + a_1q^{-1}, a_1 = -1 \tag{14}$$

$$B(q^{-1}) = b_0 + b_1q^{-1} \tag{15}$$

where $\alpha(q^{-1})$ has the coefficient α_i (i is a natural number no more than the order) and the order $n_\alpha = n_a + n_c$, $\beta(q^{-1})$ has the coefficient β_i and the order $n_\beta = n_b + n_c$.

Define

$$\begin{cases}\boldsymbol{\theta}_1 = [\alpha_1, \alpha_2, \ldots, \alpha_{n_a+n_c}, \beta_0, \beta_1, \ldots, \beta_{n_b+n_c}]\\ \boldsymbol{\varphi}_1(t) = [-u_2(t-1), \ldots, -u_2\left(t-n_\alpha\right), i_C(t), \ldots,\\ \qquad i_C\left(t-n_\beta\right)]\end{cases}. \tag{16}$$

We have

$$u_2(t) = \boldsymbol{\varphi}_1^{\mathrm{T}}(t)\boldsymbol{\theta}_1 + \varepsilon(t). \tag{17}$$

Thus, the estimation of $\boldsymbol{\theta}_1$ can be obtained by the RLS algorithm.

C. Parameter Identification of A(q^{-1}) and B(q^{-1})

The parameters in $A(q^{-1})$ and $B(q^{-1})$ can be calculated after $\alpha(q^{-1})$ and $\beta(q^{-1})$ are determined.

According to (13), we have

$$A\left(q^{-1}\right)\beta\left(q^{-1}\right) = B\left(q^{-1}\right)\alpha\left(q^{-1}\right). \tag{18}$$

Define

$$\boldsymbol{\theta}_2 = [a_1, b_0, b_1]. \tag{19}$$

We have the following incompatible linear equations:

$$\boldsymbol{G}\boldsymbol{\theta}_2 = \boldsymbol{\rho} \tag{20}$$

$$\boldsymbol{G} = \begin{bmatrix} 0 & 1 & 0\\ -\beta_0 & \alpha_1 & 1\\ -\beta_1 & \alpha_2 & \alpha_1\\ -\beta_2 & \vdots & \alpha_2\\ \vdots & \alpha_{n_\alpha} & \vdots\\ -\beta_{n_\beta} & 0 & \alpha_{n_\alpha}\end{bmatrix}, \boldsymbol{\theta}_2 = \begin{bmatrix} a_1\\ b_0\\ b_1\end{bmatrix}, \boldsymbol{\rho} = \begin{bmatrix} \beta_0\\ \beta_1\\ \beta_2\\ \vdots\\ \beta_{n_\beta}\\ 0\end{bmatrix}. \tag{21}$$

It has a least-squares (LS) solution, and $\boldsymbol{\theta}_2$ can be calculated by

$$\boldsymbol{\theta}_2 = \left(\boldsymbol{G}^{\mathrm{T}}\boldsymbol{G}\right)^{-1}\boldsymbol{G}^{\mathrm{T}}\boldsymbol{\rho}. \tag{22}$$

D. Parameter Identification of D(q^{-1})

Because

$$C\left(q^{-1}\right) = D^{-1}\left(q^{-1}\right). \tag{23}$$

We have

$$\alpha\left(q^{-1}\right)D\left(q^{-1}\right) = A\left(q^{-1}\right), \beta\left(q^{-1}\right)D\left(q^{-1}\right) = B\left(q^{-1}\right). \tag{24}$$

Then, the following incompatible linear equations can be obtained:

$$\boldsymbol{H}\boldsymbol{\theta}_3 = \boldsymbol{\delta} \tag{25}$$

$$\boldsymbol{H} = \begin{bmatrix} 1 & 0 & 0\\ \alpha_1 & 1 & 0\\ \alpha_2 & \alpha_1 & 1\\ \vdots & \alpha_2 & \alpha_1\\ \alpha_{n_\alpha} & \vdots & \alpha_2\\ 0 & \alpha_{n_\alpha} & \vdots\\ 0 & 0 & \alpha_{n_\alpha}\\ \beta_0 & 0 & 0\\ \beta_1 & \beta_0 & 0\\ \beta_2 & \beta_1 & \beta_0\\ \vdots & \beta_2 & \beta_1\\ \beta_{n_\beta} & \vdots & \beta_2\\ 0 & \beta_{n_\beta} & \vdots\\ 0 & 0 & \beta_{n_\beta}\end{bmatrix}, \boldsymbol{\theta}_3 = \begin{bmatrix} d_1\\ d_2\\ \vdots\\ d_{n_d}\end{bmatrix}, \boldsymbol{\delta} = \begin{bmatrix} a_1 - \alpha_1\\ -\alpha_2\\ \vdots\\ -\alpha_{n_\alpha}\\ 0\\ 0\\ 0\\ b_1 - \beta_1\\ -\beta_2\\ \vdots\\ \beta_{n_\beta}\\ 0\\ 0\\ 0\end{bmatrix}. \tag{26}$$

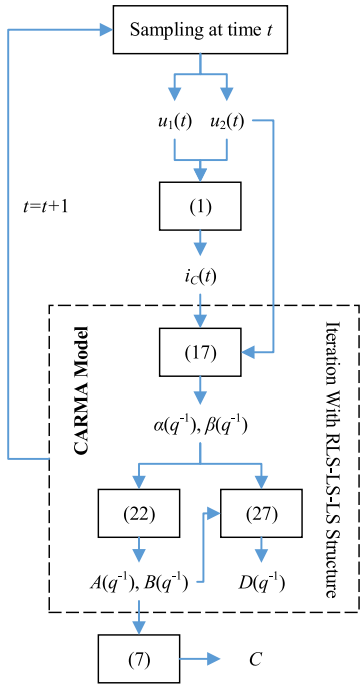

Fig. 5. Capacitance estimation process.

It also has an LS solution, and $\boldsymbol{\theta}_3$ can be calculated by

$$\boldsymbol{\theta}_3 = \left(\boldsymbol{H}^{\mathrm{T}}\boldsymbol{H}\right)^{-1}\boldsymbol{H}^{\mathrm{T}}\boldsymbol{\delta}. \tag{27}$$

Here, all parameters in (8) have been estimated, and the capacitance of the dc-link capacitor can be determined.

E. Capacitance Estimation Process

The entire capacitance estimation process is shown in Fig. 5. The voltages u_1 and u_2 are sampled when the precharging process starts. At time t, the capacitor current i_C is calculated by u_1 and u_2. Then, i_C and u_2 are used for iterative calculation. The parameters of $\alpha(q^{-1})$ and $\beta(q^{-1})$ are first estimated, and the polynomials $A(q^{-1})$, $B(q^{-1})$, and $D(q^{-1})$ are determined according to $\alpha(q^{-1})$ and $\beta(q^{-1})$. The iterative calculation repeats until the end of the precharging process, and the capacitance is determined by the final values of b_0 and b_1.

IV. Verifications and Comparisons

A. Test Preparations

The proposed method was tested on a dSPACE platform and a vehicle in Shenzhen Metro Group. The global view of the platform and the vehicle is shown in Fig. 6. The platform includes the dSPACE system (DS6001, DS6101, DS6201, DS2655, DS2655_M1, and the software), the computer and the simulation model of the precharging circuit. The working principle and all parameters of the simulation model are consistent with those of the real precharging circuit on the vehicle. In the real circuit, there are two voltage sensors (SV1 and SV2) used to measure the voltages u_1 and u_2. These two sensors belong to the original system, and the data they collect are transmitted to the onboard computer for easy download. The precharging circuit during the precharging process can be equivalent to that

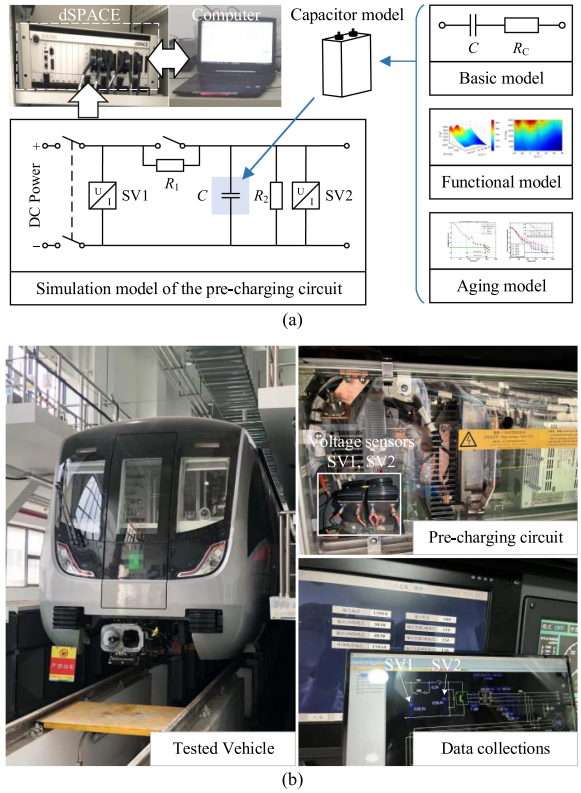

Fig. 6. dSPACE platform and tested vehicle. (a) dSPACE system and simulation models. (b) Real object and data collections.

TABLE I
Key Parameters of the Tested Vehicle

Parameters	Values
u_1	1500±10% V
C	4.4 mF
R_1	230 Ω
R_2	10 kΩ
Sampling interval	100 ms

in Fig. 4, and the key parameters of the tested vehicle are shown in Table I.

B. Verification on the Platform

The proposed method was verified on the platform, and other algorithms, such as RLS, RELS, and RSNA, were also tested for comparison. During the test, the voltage fluctuations and signal noise were added to the model to simulate actual operating conditions. Fig. 7 shows the estimated capacitance and errors. The symbol k represents the number of sampling points. The RSNA algorithm failed to estimate the capacitance, of which the error was over 66%. RLS and RELS algorithms converged rapidly but the final results were 4.572 mF and 4.574 mF, respectively. There was a bias between these estimated values and the capacitance value, and their errors were about 3.9%. Although the converging speed of the proposed method was not as good as those of RLS and RELS algorithms, the final calculation result was 4.401 mF and its accuracy reached 0.026% in the end. Therefore, the correctness of the proposed method was verified.

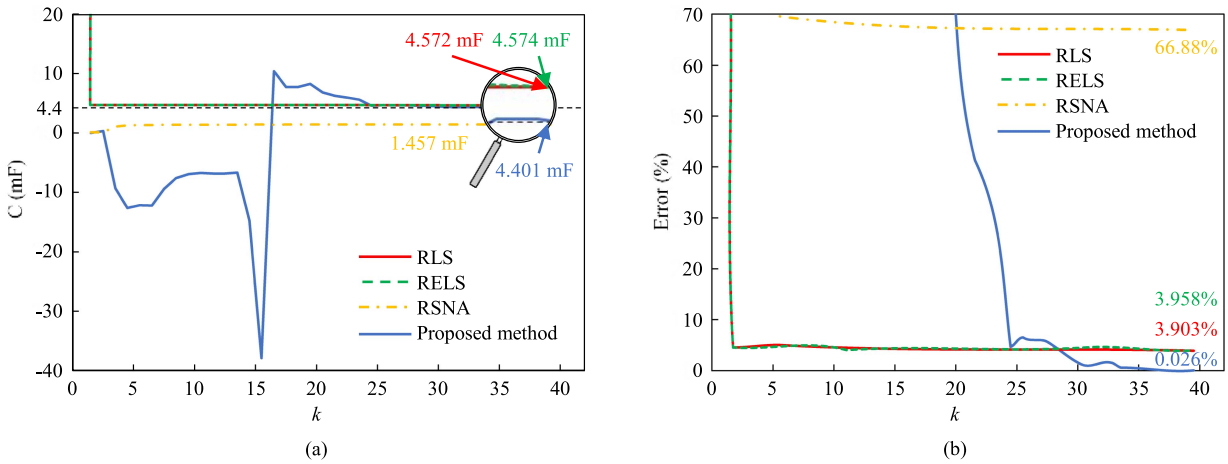

Fig. 7. Capacitance estimations and errors of different methods. (a) Capacitance estimations. (b) Estimation errors.

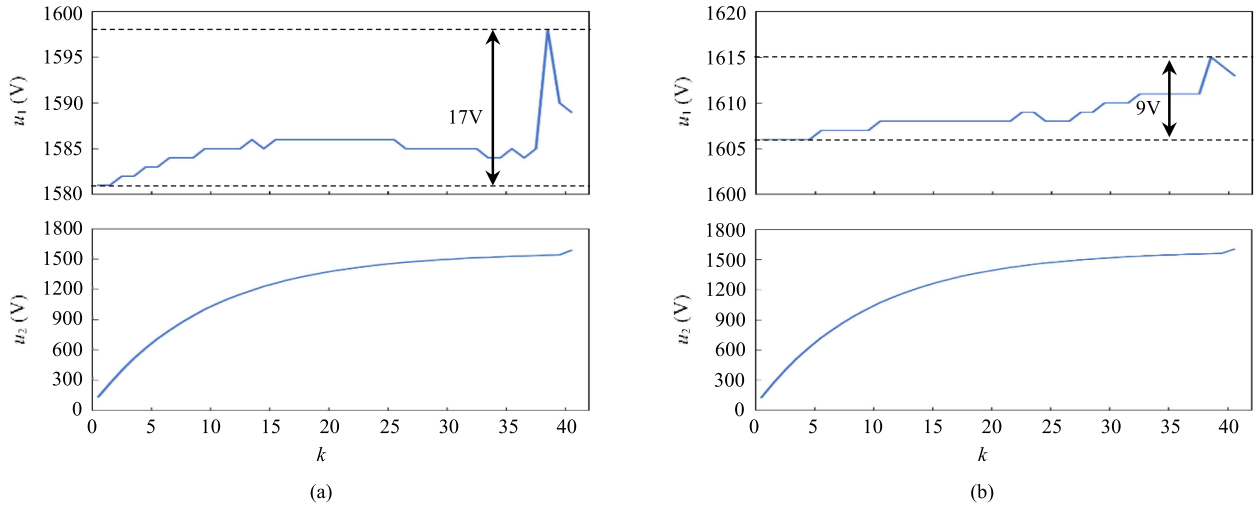

Fig. 8. Waveforms of input voltage u_1 and capacitor voltage u_2. (a) Data #1. (b) Data #2.

C. Verification on the Vehicle

The proposed method was also verified on the real vehicle. The data collection was carried out when the vehicle was in the depot and all the systems were checked normally. At the beginning of the data collection, the computer with specialized software developed by INVT Electric Company, Ltd., was connected to the system on the vehicle and the recording function was enabled. Then, the precharging circuit was connected to the input dc voltage and the capacitor voltage rose from 0 V to about 1500 V. During this period, the input dc voltage and the capacitor voltage were recorded by the computer with the sampling interval of 100 ms. The precharging circuit was disconnected with the input when the precharging and record were completed. The next record started after about 10 min, when the capacitor was fully discharged.

Two sets of the collected data named data #1 and data #2 are shown in Fig. 8. Because of the sampling interval, both the input dc voltage and the capacitor voltage only have 41 sampling points during the precharging process. It can be seen that the noise of the input voltage u_1 was also sampled, and the maximum fluctuation range captured was 17 V. Meanwhile, the input voltage u_1 was not stable and changed each time. The averages of u_1 during the precharging process were 1585 V and 1609 V, respectively. The same problem also existed in the capacitor voltage u_2, but they were not obvious because the voltage rise was large enough. Here, data #1 and data #2 are used for verifications and comparisons, because they illustrated the highest and lowest accuracy that the proposed method could achieve at that time.

Table II shows the estimation results of the proposed method when data #1 was used. The estimation results of RLS, RELS, and RSNA algorithms were also given for the comparison. When the iterative calculation was completed, the final estimated capacitance errors of RLS, RESL, RSNA, and the proposed method were 5.845%, 6.097%, 78.42%, and 0.4075%,

TABLE II
CAPACITANCE ESTIMATIONS AND ERRORS OF DIFFERENT METHODS WITH DATA #1

Methods	k								
	5	10	15	20	25	30	35	40	41
RLS	4.085 mF 7.164%	4.089 mF 7.071%	4.087 mF 7.111%	4.086 mF 7.126%	4.086 mF 7.130%	4.086 mF 7.126%	4.088 mF 7.101%	4.087 mF 7.1133%	4.143 mF 5.845%
RELS	4.090 mF 7.053%	4.086 mF 7.134%	4.087 mF 7.108%	4.086 mF 7.137%	4.086 mF 7.142%	4.086 mF 7.127%	4.087 mF 7.122%	4.087 mF 7.119%	4.132 mF 6.097%
RSNA	0.7621 mF 82.68%	0.8374 mF 80.97%	0.8497 mF 80.69%	0.8565 mF 80.53%	0.8595 mF 80.46%	0.8626 mF 80.40%	0.8639 mF 80.37%	0.8935 mF 79.69%	0.9494 mF 78.42%
The proposed method	4.399 mF 0.0073%	4.443 mF 0.9899%	4.195 mF 4.648%	4.254 mF 3.313%	4.386 mF 0.3231%	4.386 mF 0.3108%	4.380 mF 0.4538%	4.355 mF 1.033%	4.418 mF 0.4075%

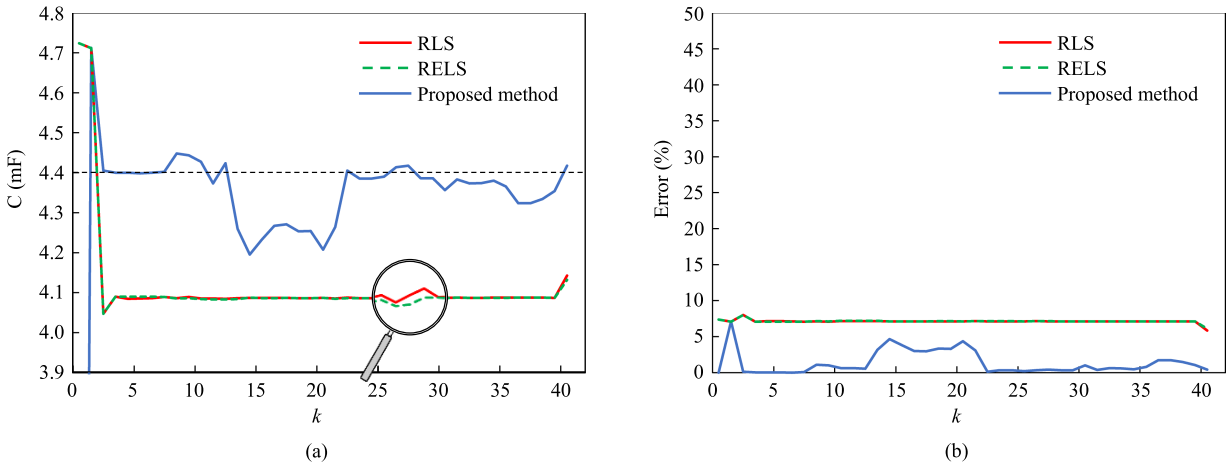

Fig. 9. Capacitance estimations and errors of different methods with data #1. (a) Capacitance estimations. (b) Estimation errors.

respectively. Due to the large sampling interval and the noise of the voltages, the RSNA algorithm failed to find the accurate solution. The RLS algorithm showed better performance than the RELS algorithm, and the proposed method achieved the best estimation result. For a detailed comparison, the entire iteration process of RLS, RELS, and the proposed method is given in Fig. 9. The black dotted line indicates the true capacitance of the capacitor. Although the RLS and RELS algorithms converged to a certain range faster, there were large constant errors between their calculation results and the true value. The main causes were the colored noise and limited sampling points. The proposed method reached the real value quickly at the beginning of the iteration but fluctuated in the middle and eventually went back to the real value. This phenomenon is mainly related to the precharging curve and the noise evaluation involved in the algorithm. At the beginning of the precharging process, the capacitor voltage rises rapidly and the voltage change is much greater than the noise variation, making it easy to obtain the accurate estimations. In the middle of the precharging process, the voltage change of the capacitor decreases while the noise impact increases relatively, and the curve of the entire precharging process has not yet formed. It may behave like another precharging curve due to the influence of noise and causes the continuous adjustment of parameter estimations. At the end of the precharging process, the entire curve is basically determined, and the proposed method can effectively evaluate the impact of noise, thereby obtaining accurate capacitance estimations.

Table III shows the estimation results of the proposed method when data #2 was used. The estimation results of RLS, RELS, and RSNA algorithms were also included. It can be seen that the final estimated capacitance errors of RLS, RESL, RSNA, and the proposed method were 5.575%, 5.679%, 80.29%, and 1.693%, respectively. The proposed method performed better than other algorithms. A detailed comparison of RLS, RELS, and the proposed method is shown in Fig. 10. Similarly, the RLS and RELS algorithms had large constant errors. The proposed method converged at the beginning, fluctuated in the middle, and returned to the real value in the end.

D. Influence of Resistance Offset

Because the parameters R_1 and R_2 are used in the algorithm, the influence of resistance offsets is studied.

Generally, it is difficult and prohibited to replace the resistors on the vehicle during the experiment. Thus, the resistance value in the algorithm was modified to test the impact of deviation between the observed and actual resistance values. Fig. 11 shows the detailed information and comparisons. When the resistance of R_1 changed, there was an approximate linear increasing relationship between the error of the proposed method and the

TABLE III
CAPACITANCE ESTIMATIONS AND ERRORS OF DIFFERENT METHODS WITH DATA #2

Methods	k								
	5	10	15	20	25	30	35	40	41
RLS	4.103 mF 6.745%	4.106 mF 6.672%	4.109 mF 6.615%	4.108 mF 6.644%	4.109 mF 6.616%	4.110 mF 6.585%	4.110 mF 6.587%	4.110 mF 6.582%	4.155 mF 5.575%
RELS	4.105 mF 6.701%	4.107 mF 6.653%	4.105 mF 6.700%	4.107 mF 6.665%	4.109 mF 6.622%	4.111 mF 6.567%	4.111 mF 6.577%	4.110 mF 6.593%	4.150 mF 5.679%
RSNA	0.7522 mF 82.90%	0.8295 mF 81.15%	0.8412 mF 80.88%	0.8478 mF 80.73%	0.8503 mF 80.67%	0.8527 mF 80.62%	0.8525 mF 80.62%	0.8530 mF 80.61%	0.8673 mF 80.29%
The proposed method	4.382 mF 0.4145%	4.251 mF 3.385%	4.272 mF 2.903%	4.275 mF 2.833%	4.183 mF 4.934%	4.181 mF 4.968%	4.097 mF 6.890%	4.015 mF 8.758%	4.474 mF 1.693%

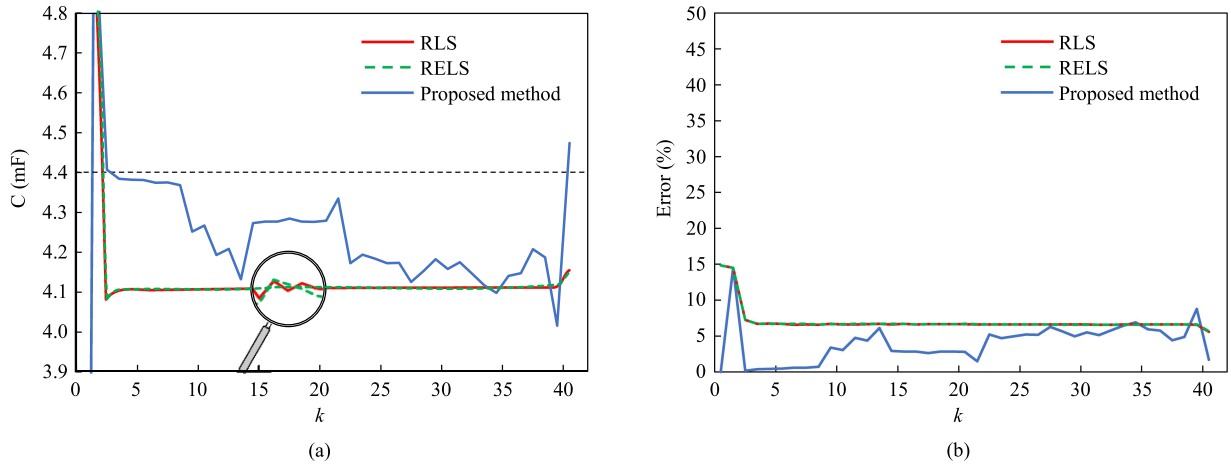

Fig. 10. Capacitance estimations and errors of different methods with data #2. (a) Capacitance estimations. (b) Estimation errors.

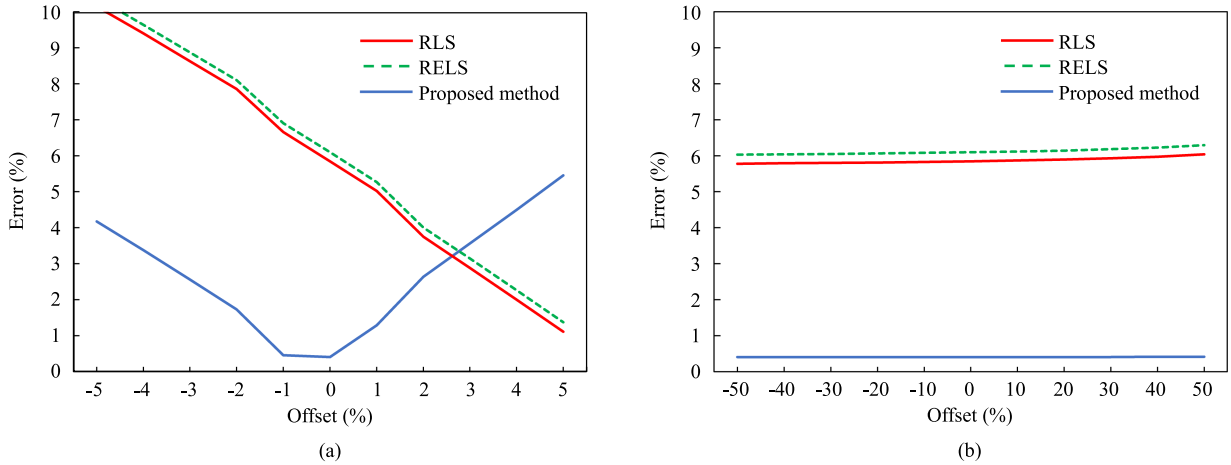

Fig. 11. Influence of resistance offset on capacitance estimation errors. (a) R_1. (b) R_2.

absolute value of the resistance offset. The error was within 2% when the offset was in the range of −2.4%–1.6%, and it reached the minimum point when the offset was zero. The errors of RLS and RELS algorithms also have the piecewise linear relationship with the resistance offset. But their minimum points showed a significant shift to the right. The resistance variation of R_2 did not have a significant impact on these algorithms. The errors of RLS, RELS, and the proposed method remained basically unchanged when the offset was 50%, but they increased greatly when the resistance was set to zero.

Although the resistance variation has an influence on the estimation errors, it is not serious in reality. The effective working time of R_1 in the circuit is very short every day, and the heat of R_2 is very small during the operation. Therefore, the degradation of R_1 or R_2 is an extremely long process, and the impact of resistor aging on the proposed method can be ignored.

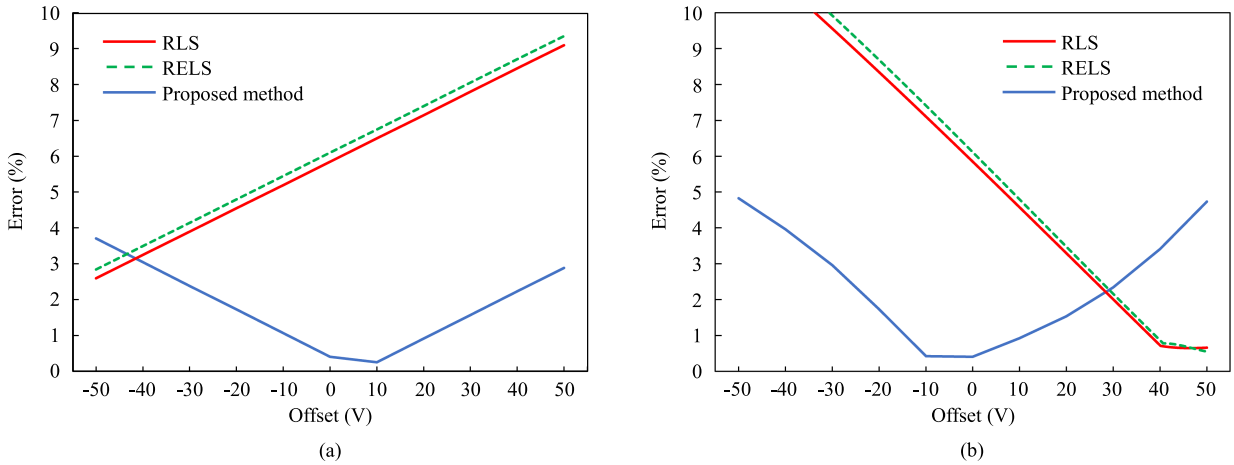

Fig. 12. Influence of the voltage signal offset on capacitance estimation errors. (a) u_1. (b) u_2.

TABLE IV
COMPARISONS WITH EXISTING METHODS

Methods	Target	Accuracy	Problem #1 solved	Problem #2 solved	Others
[9]	C, ESR	< 3%	Y	Unknown	Injected currents
[10]	C	< 5%	N	N	Injected currents
[11]	ESR	< 2%	N	N	Extra sensors and high-performance chips are required
[12]	C	< 1%	Y	N	Discharge to the motor is required
[13]	C, ESR	< 1%	N	N	–
[15]	C	< 1%	N	N	High-precise differential of the capacitor voltage is required
[16]	C	< 3%	N	N	–
[18]	C, ESR	< 10%	Y	Unknown	–
[19]	C, ESR	< 1%	N	N	–
[28]	ESR	< 10%	N	N	–
[30]	ESR	< 7%	N	N	–
[33]	C	< 4%	Y	N	Control signals for current calculation are required
[34]	ESR	< 4%	N	N	–
[35]	C	< 1%	N	N	Control strategy modification, parameters of the *LC* filter and the motor are required
[36]	C	< 3%	Y	N	Load current sensor is required
[37]	C	< 3.5%	Y	N	–
The proposed method	C	< 2%	Y	Y	–

Note: Problem #1 is the large estimation errors caused by voltage sensor noise, and problem #2 is the low accuracy caused by the sampling interval of 100 ms.

Meanwhile, the maintenance personnel will regularly check and record the values of these resistors to ensure the resistor value in a tolerable range. For example, in metro applications, the resistors are tested every 5 years and replaced with the same one when the value is out of the range. The resistance values in the algorithm can also be updated after the regular check to ensure the estimation accuracy as much as possible.

E. Influence of Voltage Signal Offset

In harsh working environments, voltage sensors may fail and lead to the signal offset. Thus, the influence of the voltage signal offset was also studied in this article. For each signal, the signal offset was simulated by adding the constant value to the original signal.

Fig. 12 shows the performance of RLS, RELS, and the proposed method with different signal offsets. For the proposed method, the error has an approximate linear increasing relationship with the absolute value of the voltage signal offset. It was within 2% when the offset of u_1 was in the range of -25 to 36 V or the offset of u_2 was in the range of -22 to 26 V. For the RLS and RELS algorithms, the errors have the piecewise linear relationship with the signal offset. The minimum points shifted to the left when the offset existed in u_1 or right in u_2.

In comparison, the proposed method has better signal-offset immunity and can work well even in the case of slight sensor failures.

F. Comparison With Existing Methods

The comparison with existing methods is shown in Table IV, which mainly includes the estimation target, the accuracy, and two problems mentioned in Section I. Because the equivalent series resistance (ESR) in the DC-link capacitors is not the same as that of electrolytic capacitors, and has less impact on the service performance the proposed method only focuses on the estimation of capacitance. The ESR of the dc-link capacitors can be calculated by (6) as well. The accuracy of these methods varies from 1% to 10% and that of the proposed method is within 2%. For the most important problems that exist in railway applications, less than half of the methods are able to get good estimation results with poor signals, and few methods demonstrate the practicality with extremely low sampling frequency. Although each method has its own characteristics and application, the comparison shows that the method proposed in this article is more suitable for railway applications.

V. Conclusion

Focusing on the problems of capacitor condition monitoring in railway applications, a capacitance estimation method based on the precharging model and low sampling frequency is proposed. The precharging model can effectively eliminate the impact of voltage sensor noise, which may bring huge errors to existing methods. Meanwhile, the three-stage estimation algorithm also reduces the noise influence and is able to find the optimal solution with extremely low sampling frequency. Accurate estimation results can be obtained with the input dc voltage and the capacitor voltage, and extra modifications to the system are not required.

The proposed method was verified on a vehicle, and the estimation error is within 2%, which is superior to those of RLS, RELS, and RSNA algorithms. Moreover, the proposed method has immunity to a certain degree of resistance offset and voltage signal offset, and the comparison with existing methods also shows that the method proposed in this article is more suitable for railway applications.

References

[1] Z. Zhao, P. Davari, W. Lu, H. Wang, and F. Blaabjerg, "An overview of condition monitoring techniques for capacitors in DC-link applications," *IEEE Trans. Power Electron.*, vol. 36, no. 4, pp. 3692–3716, Apr. 2021, doi: 10.1109/TPEL.2020.3023469.

[2] C. Lv, J. Liu, Y. Zhang, W. Lei, and R. Cao, "An improved lifetime prediction method for metallized film capacitor considering harmonics and degradation process," *Microelectronics Rel.*, vol. 114, Oct. 2020, Art. no. 113892, doi: 10.1016/j.microrel.2020.113892.

[3] X. Wu et al., "A capacitance estimation method for DC-link capacitors based on pre-charging model and noise evaluation," *IEEE Trans. Ind. Electron.*, vol. 70, no. 8, pp. 8477–8487, Aug. 2023, doi: 10.1109/TIE.2022.3217587.

[4] C. Shu et al., "Residual lifetime prediction of metallized film capacitors based on feature extraction and error compensation," *Proc. Civil, Struct., Environ. Eng.*, vol. 42, no. 7, pp. 2670–2680, Apr. 2022, doi: 10.13334/j.0258-8013.pcsee.210278.

[5] A. El Mejdoubi, H. Chaoui, J. Sabor, and H. Gualous, "Remaining useful life prognosis of supercapacitors under temperature and voltage aging conditions," *IEEE Trans. Ind. Electron.*, vol. 65, no. 5, pp. 4357–4367, May 2018, doi: 10.1109/TIE.2017.2767550.

[6] H. Wang, P. Davari, H. Wang, D. Kumar, F. Zare, and F. Blaabjerg, "Lifetime estimation of DC-link capacitors in adjustable speed drives under grid voltage unbalances," *IEEE Trans. Power Electron.*, vol. 34, no. 5, pp. 4064–4078, May 2019, doi: 10.1109/TPEL.2018.2863701.

[7] X. Wang, B. Jiang, S. X. Ding, N. Lu, and Y. Li, "Extended relevance vector machine-based remaining useful life prediction for DC-link capacitor in high-speed train," *IEEE Trans. Cybern.*, vol. 52, no. 9, pp. 9746–9755, Sep. 2022, doi: 10.1109/TCYB.2020.3035796.

[8] G. Liu et al., "Life prediction of capacitor based on AVC by ESM-BP hybrid neural network model," in *Proc. 7th Int. Conf. Elect. Electron. Eng.*, 2020, pp. 61–66.

[9] N. Agarwal, M. W. Ahmad, and S. Anand, "Quasi-online technique for health monitoring of capacitor in single-phase solar inverter," *IEEE Trans. Power Electron.*, vol. 33, no. 6, pp. 5283–5291, Jun. 2018, doi: 10.1109/TPEL.2017.2736162.

[10] T. Li, J. Chen, P. Cong, X. Dai, R. Qiu, and Z. Liu, "Online condition monitoring of DC-link capacitor for AC/DC/AC PWM converter," *IEEE Trans. Power Electron.*, vol. 37, no. 1, pp. 865–878, Jan. 2022, doi: 10.1109/TPEL.2021.3092429.

[11] D. Xiang, Y. Zheng, H. Li, Y. Gu, N. Zhao, and J. Zheng, "Online ESR monitoring of DC-link capacitor in voltage-source-converter using damping characteristic of switching ringings," *IEEE Trans. Power Electron.*, vol. 36, no. 7, pp. 7429–7441, Jul. 2021, doi: 10.1109/TPEL.2020.3042218.

[12] H. Li, D. Xiang, X. Han, X. Zhong, and X. Yang, "High-accuracy capacitance monitoring of DC-link capacitor in VSI systems by LC resonance," *IEEE Trans. Power Electron.*, vol. 34, no. 12, pp. 12200–12211, Dec. 2019, doi: 10.1109/TPEL.2019.2904551.

[13] B. Wang, J. Meng, and P. Zhao, "Aging condition monitoring for aluminum electrolytic capacitor in variable speed drives," *IEEE Trans. Power Electron.*, vol. 37, no. 4, pp. 4564–4574, Apr. 2022, doi: 10.1109/TPEL.2021.3121813.

[14] F. Deng et al., "Capacitor ESR and *C* monitoring in modular multilevel converters," *IEEE Trans. Power Electron.*, vol. 35, no. 4, pp. 4063–4075, Apr. 2020, doi: 10.1109/TPEL.2019.2939185.

[15] N. Zhao, R. Gao, G. Wang, D. Ding, G. Zhang, and D. Xu, "Online estimation method of DC-link capacitors for reduced DC-link capacitance IPMSM drives," *IEEE Trans. Power Electron.*, vol. 36, no. 11, pp. 12196–12201, Nov. 2021, doi: 10.1109/TPEL.2021.3079476.

[16] M. W. Ahmad, P. N. Kumar, A. Arya, and S. Anand, "Noninvasive technique for DC-link capacitance estimation in single-phase inverters," *IEEE Trans. Power Electron.*, vol. 33, no. 5, pp. 3693–3696, May 2018, doi: 10.1109/TPEL.2017.2762341.

[17] Y. Gupta, M. W. Ahmad, S. Narale, and S. Anand, "Health estimation of individual capacitors in a bank with reduced sensor requirements," *IEEE Trans. Ind. Electron.*, vol. 66, no. 9, pp. 7250–7259, Sep. 2019, doi: 10.1109/TIE.2018.2880725.

[18] Z. Zhao, W. Lu, P. Davari, X. Du, H. H.-C. Iu, and F. Blaabjerg, "An online parameters monitoring method for output capacitor of buck converter based on large-signal load transient trajectory analysis," *IEEE J. Emerg. Sel. Topics Power Electron.*, vol. 9, no. 4, pp. 4004–4015, Aug. 2021, doi: 10.1109/JESTPE.2020.2964068.

[19] P. Sundararajan et al., "Condition monitoring of DC-link capacitors using Goertzel algorithm for failure precursor parameter and temperature estimation," *IEEE Trans. Power Electron.*, vol. 35, no. 6, pp. 6386–6396, Jun. 2020, doi: 10.1109/TPEL.2019.2951859.

[20] Y. Zhao et al., "Structure and parameter identification of supercapacitors based on particle swarm optimization," *Proc. Civil, Struct., Environ. Eng.*, vol. 32, no. 15, pp. 155–161, 2012.

[21] S. Cheng et al., "An on-line capacitor state identification method based on improved RLS," *Transp. Saf. Environ.*, vol. 3, no. 3, pp. 1–13, May 2021, doi: 10.1093/tse/tdab007.

[22] K. Wang, L. Jin, G. Li, Y. Deng, and X. He, "Online capacitance estimation of submodule capacitors for modular multilevel converter with nearest level modulation," *IEEE Trans. Power Electron.*, vol. 35, no. 7, pp. 6678–6681, Jul. 2020, doi: 10.1109/TPEL.2019.2959074.

[23] M. Asoodar, M. Nahalparvari, C. Danielsson, R. Söderström, and H.-P. Nee, "Online health monitoring of DC-link capacitors in modular multilevel converters for FACTS and HVDC applications," *IEEE Trans. Power Electron.*, vol. 36, no. 12, pp. 13489–13503, Dec. 2021, doi: 10.1109/TPEL.2021.3091780.

[24] W. Xun et al., "Pre-charging model based capacitance estimation method for DC-link capacitors with low sampling frequency," *J. Central South Univ. (Sci. Technol.)*, vol. 54, no. 8, pp. 3325–3334, 2023, doi: 10.11817/j.issn.1672-7207.2023.08.033.
[25] C. Li, Y. Yu, Z. Yang, Q. Liu, and X. Peng, "ESR estimation for aluminum electrolytic capacitor of power electronic converter based on compressed sensing and wavelet transform," *IEEE Trans. Ind. Electron.*, vol. 69, no. 2, pp. 1948–1957, Feb. 2022, doi: 10.1109/TIE.2021.3055164.
[26] L. Ren and C. Gong, "Online estimation scheme of output capacitor's ESR and tanδ for buck converter," *Inst. Eng. Technol. Power Electron.*, vol. 12, no. 11, pp. 2978–2986, 2019, doi: 10.1049/iet-pel.2018.5394.
[27] L. Ren, C. Gong, and Y. Zhao, "An online ESR estimation method for output capacitor of boost converter," *IEEE Trans. Power Electron.*, vol. 34, no. 10, pp. 10153–10165, Oct. 2019, doi: 10.1109/TPEL.2018.2890617.
[28] W. Lu, X. Lu, J. Han, Z. Zhao, and X. Du, "Online Estimation of ESR for DC-link capacitor of boost PFC converter using wavelet transform based time–frequency analysis method," *IEEE Trans. Power Electron.*, vol. 35, no. 8, pp. 7755–7764, Aug. 2020, doi: 10.1109/TPEL.2019.2957027.
[29] K. Laadjal, M. Sahraoui, and A. J. M. Cardoso, "On-line fault diagnosis of DC-link electrolytic capacitors in boost converters using the STFT technique," *IEEE Trans. Power Electron.*, vol. 36, no. 6, pp. 6303–6312, Jun. 2021, doi: 10.1109/TPEL.2020.3040499.
[30] Y. Zhang, Z. Lian, W. Fu, and X. Chen, "An ESR quasi-online identification method for the fractional-order capacitor of forward converters based on variational mode decomposition," *IEEE Trans. Power Electron.*, vol. 37, no. 4, pp. 3685–3690, Apr. 2022, doi: 10.1109/TPEL.2021.3119966.
[31] D. Ronanki and S. S. Williamson, "Failure prediction of submodule capacitors in modular multilevel converter by monitoring the intrinsic capacitor voltage fluctuations," *IEEE Trans. Ind. Electron.*, vol. 67, no. 4, pp. 2585–2594, Apr. 2020, doi: 10.1109/TIE.2019.2912771.
[32] E. R. Ramos, R. Leyva, G. G. Farivar, C. D. Townsend, and J. Pou, "Capacitor condition monitoring for the low-capacitance statcom: An online approach," *IEEE Trans. Power Electron.*, vol. 37, no. 4, pp. 3697–3701, Apr. 2022, doi: 10.1109/TPEL.2021.3120493.
[33] F. Yao et al., "Parameter identification of DC-link capacitor for electric vehicle based on IGWO-BP neural network," *IEEJ Trans. Elect. Electron. Eng.*, vol. 16, pp. 861–870, 2021, doi: 10.1002/tee.23373.
[34] P. Sundararajan, M. H. M. Sathik, F. Sasongko, C. S. Tan, M. Tariq, and R. Simanjorang, "Online condition monitoring system for DC-link capacitor in industrial power converters," *IEEE Trans. Ind. Appl.*, vol. 54, no. 5, pp. 4775–4785, Sep./Oct. 2018, doi: 10.1109/TIA.2018.2845889.
[35] T. Meng and P. Zhang, "An online DC-link capacitance estimation method for motor drive systems based on an intermittent reverse-charging control strategy," *IEEE Trans. Power Electron.*, vol. 38, no. 2, pp. 2481–2492, Feb. 2023, doi: 10.1109/TPEL.2022.3211314.
[36] Z. Zhao, P. Davari, Y. Wang, and F. Blaabjerg, "Online capacitance monitoring for DC/DC boost converters based on low-sampling-rate approach," *IEEE J. Emerg. Sel. Topics Power Electron.*, vol. 10, no. 5, pp. 5192–5204, Oct. 2022, doi: 10.1109/JESTPE.2021.3108420.
[37] Z. Zhao, P. Davari, W. Lu, and F. Blaabjerg, "Online DC-link capacitance monitoring for digital-controlled boost PFC converters without additional sampling devices," *IEEE Trans. Ind. Electron.*, vol. 70, no. 1, pp. 907–920, Jan. 2023, doi: 10.1109/TIE.2022.3153825.

Xun Wu (Member, IEEE) was born in Xinhua, China, in 1993. He received the B.E. degree in electrical engineering and the Ph.D. degree in traffic information engineering and control from Central South University, Changsha, China, in 2015 and 2019, respectively.

From 2018 to 2019, he was a Visiting Scholar with California PATH, UC Berkeley, CA, USA. He is currently a Lecturer with the School of Traffic & Transportation Engineering, Central South University. His research interests include fault diagnosis and control techniques of power electronic converters, condition monitoring and life prediction of capacitors, and safety analysis.

Kaidi Li was born in Nanning, China, in 1992. He received the B.E. degree in electrical engineering from the Changsha University of Science and Technology, Changsha, China, in 2013, and the M.S. degree in electrical engineering and the Ph.D. degree in traffic equipment and information engineering both from Central South University, Changsha, in 2016 and 2019, respectively.

He is currently with Shenzhen Metro Group Company, Ltd., Shenzhen, China. His main research areas include fault diagnosis and fault-tolerant control of power electronic converters.

Rui Tian was born in Fenyang, China, in 1992. She received the B.E. and M.S. degrees in electrical engineering from Central South University, Changsha, China, in 2015 and 2018, respectively.

She is currently with State Grid Hunan Extra High Voltage Substation Company, Changsha. Her research interests include fault diagnosis of power electronic converters and transformers.

Hengyi Yin was born in Changsha, China, in 2002. He is currently working toward the B.E. degree in electrical engineering from McGill University, Montréal, QC, USA.

In 2023, he engaged in research focused on the condition monitoring of dc-link capacitors. His current research interests include power electronics and dc-link capacitor modeling.

Tianjian Yu received the Ph.D. degree in traffic equipment and information engineering from Central South University, Changsha, China, in 2017.

Since 2014, he has been a Visiting Ph.D. Student with the University of Pittsburgh, Pittsburgh, PA, USA. He is currently an Associate Professor with the School of Traffic & Transportation Engineering, Central South University. His research interest includes fault diagnosis of traffic equipment, in particular on bearings and inverters.

Shu Cheng was born in Changsha, China, in 1981. He received the B.E. degree in automation from the East China University of Science and Technology, Shanghai, China, in 2003, and the M.S. and Ph.D. degrees in electrical engineering from Central South University, Changsha, in 2006 and 2011, respectively.

Since 2007, he has been a permanent Researcher with the Institute of Rail Transport and Electric Traction Technology, Central South University. He is currently a Professor with the School of Traffic & Transportation Engineering, Central South University. His research interests include fault diagnosis and fault-tolerant control of electrical drivers and electric traction control technology.

Chunyang Chen was born in Nanling, China, in 1962. He received the B.E. degree in electric locomotive from Southwest Jiaotong University, Chengdu, China, in 1983, the master's degree from Hunan University, Changsha, China, in 1999, and the Ph.D. degree from Beijing Jiaotong University, Beijing, China, in 2008.

He was the Deputy Director of Science and Technology Department, Ministry of Railways, the President of Southwest Jiaotong University, and the Vice-President of Central South University. His research interests include the electric locomotive and intelligent transportation systems.